Modeling of Cluster's electric antennas in space: Application to plasma diagnostics

C. Béghin,[1] P. M. E. Décréau,[1] J. Pickett,[2] D. Sundkvist,[1,3] and B. Lefebvre[4,5]

Received 9 March 2005; revised 16 June 2005; accepted 28 June 2005; published 24 November 2005.

[1] The main characteristics of the long-boom electric antennas installed on board the Cluster satellites are derived from finite element modeling in a kinetic and isotropic space plasma, in the frequency range of about 1–100 kHz. The model is based on the surface charge distribution method in quasi-static conditions. The impedances of both types of antenna, i.e., the double-wire and the double-probe, are computed versus the frequency normalized with respect to the local plasma frequency and for several different Debye lengths. Most of the code outputs are checked using analytic estimations for better understanding of the involved physical mechanisms. As a by-product, the effective length of the double-probe antenna and the mutual impedance between the two antennas are computed by the code. It is shown that if it had been possible to implement such measurements on board, one would have been able not only to determine accurately the electric characteristics of the antennas but also to estimate the local plasma parameters. Nevertheless, an interesting feature predicted by the model has been checked recently in orbit by running a special mode of operation for testing the mutual impedance measurement. The preliminary results are globally consistent with the predictions, except that they suggest that our Maxwellian model for the electron distribution should be revised in order to explain the unexpected low-frequency response. After analysis of the electron flux measurements obtained simultaneously, it appears that a rough adjustment of the electron distribution with a two-component distribution allows us to account for the observations.

Citation: Béghin, C., P. M. E. Décréau, J. Pickett, D. Sundkvist, and B. Lefebvre (2005), Modeling of Cluster's electric antennas in space: Application to plasma diagnostics, *Radio Sci.*, *40*, RS6008, doi:10.1029/2005RS003264.

1. Introduction

[2] Each of the four satellites of the Cluster space fleet carries a pair of mutually perpendicular long-boom antennas with spherical probes at their tips, each about 88 m tip to tip, located in the spin plane [*Gustafsson et al.*, 1997]. Several wave experiments use these antennas at different frequencies, ranging from direct current up to about 580 kHz in passive as well as active modes of operation, within a coordinated consortium [*Pedersen et al.*, 1997]. Since the behavior of such antennas is known to depend strongly on the frequency, their design is quite sophisticated in order to comply with the constraints of each experiment. For the modeling of the antenna in terms of finite elements as presented here, we tried to follow the real structure as closely as possible. This study applies to a so-called "high-frequency" (HF) range, from a few kilohertz up to about 100 kHz, a wide band which includes the local plasma frequency along the Cluster orbit. We will ignore the influence of the ions on the waves in this range, and we will neglect the anisotropy due to the steady magnetic field whenever the electron cyclotron frequency lies well below the plasma frequency. This contrasts with the quite different antenna behavior in the near-zero and ULF ranges, which have their own constraints mainly dominated by the magnetic field and the conductivity of the ambient plasma, including the current of photoelectrons escaping from

[1]Laboratoire de Physique et Chimie de l'Environnement, Centre National de la Recherche Scientifique, Université d'Orléans, Orléans, France.
[2]Department of Physics and Astronomy, University of Iowa, Iowa City, Iowa, USA.
[3]On leave from Swedish Institute of Space Physics, Uppsala, Sweden.
[4]Queen Mary University of London, London, UK.
[5]Now at Blackett Laboratory, Imperial College London, London, UK.

0048-6604/05/2005RS003264

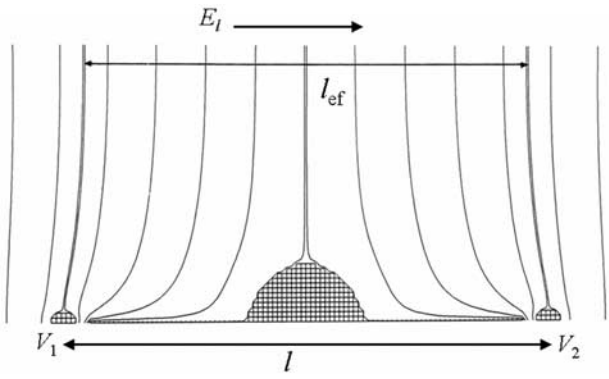

Figure 1. Free space distribution of equipotential surfaces associated with the component E_l of a uniform external electric field in the vicinity of a rough model of the S/C with a double-sphere dipole lying along the direction of the field.

the Sun-exposed spacecraft (S/C) surfaces [*Pedersen et al.*, 1998].

[3] In the above defined HF domain the ambient medium must be considered as a dielectric with a frequency-dependent permittivity, which includes the losses due to the radiation of kinetic waves from every conducting surface in contact with the plasma [*Béghin and Kolesnikova*, 1998]. The usual zero-order approximation to the basic theory for antennas shorter than the electromagnetic (EM) wavelengths consists of attributing to the ambient medium the scalar permittivity ε_0 of free space, or possibly the tensor permittivity of a cold plasma. In these conditions, most experimenters assume that the effective length of a dipole antenna is its tip-to-tip length in the case of a double sphere (or double probe) and half this length for a double wire; here the term "probe" signifies a sphere together with its connecting wire if this wire is not shielded in any way. In some cases, a more or less arbitrary correction factor is introduced to take account of the disturbances in the electrostatic field near to the spacecraft (Figure 1) and perhaps also of the noninfinite input impedance of the receiver.

[4] The above approximations can lead to significant errors in the interpretation of received signals, especially at frequencies close to plasma resonances whenever critical parameters, such as the ratio between the local Debye length and the system size, are underestimated (see, e.g., review by *Béghin* [2002]). This will be shown in more detail in section 4.3 in the specific case of Cluster for typical plasma conditions encountered along the orbit. First, we summarize the general context in which our modeling method is applicable, then we give the results of the calculation for the effective antenna length and of the simulation for various active modes of operation that the present hardware design unfortunately does not allow to be put into practice. As shown by our study, the complex behavior of such antennas could indeed be understood more easily by using a combination of active modes such as self-impedance and mutual impedance measurements. Finally, we give the results of a preliminary test of the mutual impedance measurement which has been done recently between the long-boom dipole and the double-probe antenna by coordinated simultaneous operations of the relaxation sounder Wave of High frequency and Sounder for Probing of Electron density by Relaxation (WHISPER) [*Décréau et al.*, 1997] and the waveform receiver Wide Band Data instrument(WBD) [*Gurnett et al.*, 1997]. This test validated our modeling, though the results are somewhat more complicated than we predicted initially with a single Maxwellian electron distribution. In our view, such a measurement can be regarded as an in-flight calibration of the Cluster antennas and also as a promising complementary method of plasma diagnostics.

2. Baseline

[5] In our kinetic treatment the plasma permittivity is described by the Vlasov theory using the quasi-static approximation [*Béghin*, 1995]. We consider conditions where the EM wavelength in the above defined HF range is indeed always much larger than the device size, so the quasi-static approximation is fully applicable. In an isotropic plasma the refractive index of the ordinary mode is always smaller than unity. Therefore, in the particular case of Cluster, with an upper frequency around 100 kHz, the EM wavelength can never be less than the smallest vacuum wavelength, i.e., at least 3 km, which is 30 times larger than the overall S/C size. In our model the plasma is assumed to be steady, uniform, and isotropic. The acting particles under consideration are only thermal electrons, and in its present state of development our numerical code is designed for a single Maxwellian distribution only. However, the kinetic theory allows us to introduce a combination of such distributions in order to fit any kind of distribution, provided that this remains stable enough to again use a linear approach to the problem. While awaiting a next improvement of our code including this possibility, we are proposing an analytic approximation with a two-component distribution for the interpretation of the aforementioned flight test (section 5). Similarly, the effect of a plasma drift may be significant in some occasions, as, for instance, in the second pass of the test flight. This effect can be evaluated occasionally according to a method proposed by *Kolesnikova and Béghin* [2001], but it will be not introduced in our preliminary interpretation. It is nevertheless one of the future

improvements that we intend to introduce progressively in the code.

[6] The key parameters are the plasma frequency and the Debye length which must remain within certain boundaries in order to comply with the constraints of our model. Our model in its present state of development does not include any ion sheath or photoelectron cloud around the structure, and we assume the plasma to be uniform and isotropic everywhere. We believe, however, that the ion sheath can be reasonably forgotten whenever the Debye length is at least of the same order of magnitude or larger than the cross section of the considered device. In the particular case of Cluster this can be easily satisfied for the antenna itself and marginally for the S/C body whenever the Debye length is larger than $\sim$1 m. However, secondary effects around the S/C body, as well as the wake in the case of high plasma bulk velocity, would have to be considered on some occasions. These are not included in our model, but we think that the ratio between the dipole length and the size of the S/C structure is large enough to minimize the above effects. This assumption is clearly supported by our results which are not affected significantly when we make a radical change to the shape and size of the S/C body (section 3). Moreover, as long as the density of the ambient plasma is greater than that of photoelectrons inside a sphere with a diameter of the order of the tip-to-tip antenna length, we may neglect the photoelectrons.

[7] The last major constraint applies for the value of the plasma frequency, which must be at least 3 or 4 times larger than the electron cyclotron frequency in order to satisfy a first-order approximation of quasi-isotropy. Along the Cluster orbit this condition may be not satisfied everywhere, so the results of our modeling cannot be extrapolated easily in those regions where the magnetic field is strong. There are several studies related to the behavior of electric antennas and impedance probes in magnetized plasma which could be applicable under such conditions (see, e.g., review by *Storey* [1998]). For instance, in the case of mutual impedance experiments on board the GEOS and Viking satellites, when the condition of quasi-isotropy was not satisfied in some portions of the orbit, valuable measurements of electron density and temperature might nevertheless be obtained using the hydrodynamic approach in magnetized plasma [*Décréau et al.*, 1978; *Perraut et al.*, 1990]. Although the complex full kinetic treatment in magnetized plasma could be considered, it is unlikely to be achieved in the near future; we will show in section 5 that the isotropic approximation remains valid under conditions similar to those of our test in orbit.

[8] Each conducting surface of the entire system is supposed to reach an electric equilibrium imposed by the reaction of the plasma to an external electric field or to an internal source of voltage or current, taking into account the constraints imposed by the internal connections between these surfaces. We use a conventional equivalent circuit for each component of the device that can be considered as an antenna, namely, the outer shields of the long wire booms and the terminal probes. By definition, the transfer function of an antenna in the presence of an external electric field is given by

$$V_{in} = E_l \; l^0_{ef} \frac{Z_{in}}{Z_a + Z_{in}}, \tag{1}$$

where V_{in} is the voltage at the receiver input, E_l is the component of the undisturbed electric field along the antenna axis (Figure 1), l^0_{ef} is the effective length of the antenna on open circuit, and Z_{in} and Z_a are the input impedance of the receiver and the self-impedance of the antenna, respectively.

[9] Such a conventional description is applicable obviously to any complex system as well as to an antenna in a plasma, but equation (1), which seems quite simple, becomes much more complex when both the effective length and the antenna impedance depend on several parameters such as frequency, electron density, and electron temperature. So far, most authors have used drastic approximations to obtain rough estimates of the transfer function. It must be pointed out in particular that the effective length on an open circuit depends essentially on the current distribution induced along the surface, a distribution that depends on the geometry as well as on the properties of the medium. In the simplest case of a long wire the assumption of a triangular distribution is widely used, even though it is known not to be always valid.

[10] In our approach, the above questions are bypassed because our modeling method yields a self-consistent solution for the equations of electric equilibrium, whatever the plasma conditions may be. In particular, the true charge and current distributions are computed so as to satisfy this equilibrium, taking into account the boundary conditions. Thus we can define an "acting effective length," leading directly to a simplified transfer function, the expression for which is

$$V_{in} = E_l \, l_{ef}, \tag{2}$$

where l_{ef} is the acting effective length, which now includes the load on the antenna due to the preamplifier input impedance.

[11] As we will see in section 4, besides the effective length which is essential for the interpretation of natural emissions, the model enables us to compute the self-impedance of each component of the device, as well as the mutual impedance between different components. In this way we can confirm (section 4.3) the coherence of the results derived directly from (2) using those obtained by (1), where each quantity is evaluated independently.

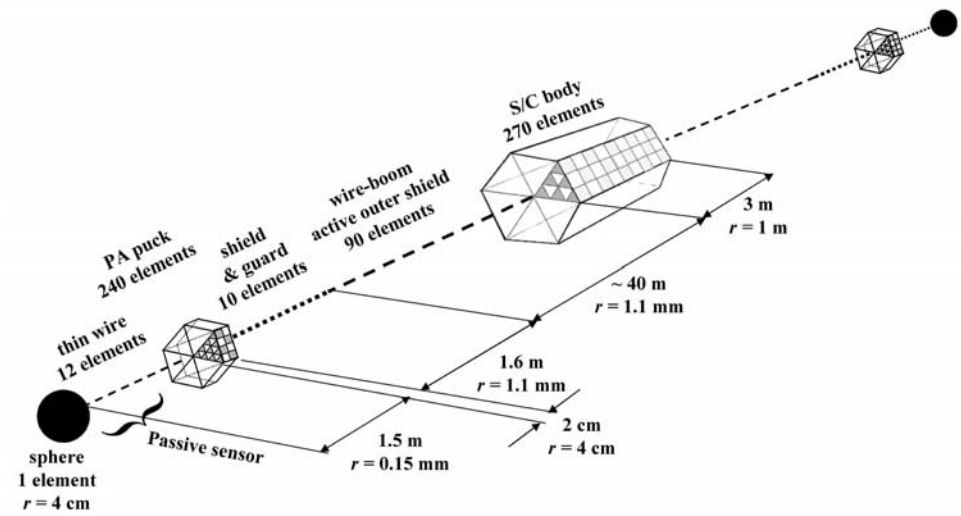

Figure 2. Model of Cluster S/C equipped with one wire boom antenna (83 m tip to tip) and one double-probe antenna (88 m tip to tip), the whole split up into 960 finite elements (not to scale).

In fact, most of the code outputs can be validated by comparing them to a simplified analytic approach so as to check the orders of magnitude and to reveal some interesting physical processes.

3. Surface Charge Distribution Method

[12] The complex layout of the dipole antennas of Cluster has been adapted to a generalized simulation code which has been developed recently at the Laboratoire de Physique et Chimie de l'Environnement, Orléans, France (P. Archambault, unpublished memorandum, 2003). The modeling, which is an application of the surface charge distribution (SCD) method proposed by *Béghin and Kolesnikova* [1998], consists first of splitting up the conducting surface of each individual part of the device, including the S/C body, into finite elements in order to follow the real shape as closely as possible, at least for the conducting parts. In order to make the model simpler we assume that the system possesses an axial revolution symmetry by steps of 60° and a global symmetry with respect to the central body (Figure 2), though the model is really three-dimensional. The sizes of the elements are adapted to each part of the device in order not only to fit the real shape but also to allow us to consider each of them as a point-like pulsating charge seen by all the others. For each monopole, going from the S/C body outward, the considered conducting parts are successively the wire boom (~40 m long), which is the active outer shield of the cables running out to the preamplifier and is used as one half of the transmitting dipole antenna for WHISPER; the guard (1.6 m long), which is a passive outer shield; the outer case of the preamplifier, which is hereinafter referred to as the "puck"; and the probe, consisting of the thin wire (1.5 m long) plus the terminal sphere (8 cm diameter), which is used as one half of the double-probe dipole. Thus the tip-to-tip antenna length is ~88 m in our model, as it actually is on Cluster (A. Eriksson, private communication, 2004). The S/C structure is taken as the reference, and at HF the pucks as well as the guards are considered to be grounded to that structure through large capacitances.

[13] The finite elements of each considered surface have different shapes depending on where they are located, but their overall dimensions must always be shorter than the Debye length. For instance, thin cables are split into small portions of cylinders a few tens of centimeters long. Because of the axial revolution symmetry of the model the S/C body cannot have its real shape. It is replaced by a hexagonal prism (3 × 2 m) made of 54 equilateral triangles on each base and 27 square elements on each face (Figure 2). However, as long as we consider modes of operation in a dipole layout, the shape of the central body does not matter because the return currents of each monopole are flowing through the reference body in opposite directions. This supposition has been checked by running the code with the S/C body reduced to a thin cylinder of radius 10 cm instead of 1 m, keeping the physical length of 3 m in order to simulate the actual gap between the feed points of the two wire booms. All results are practically unchanged, except that a slight difference, no more than ~1%, appears in the kinetic resistance of the wire boom

dipole. We believe that the same supposition would apply to the influence of the other long-boom antenna perpendicular to the one we are modeling. This would be also likely true for the short solid booms carrying the magnetometer experiments, which can be considered as an additional part of the S/C ground. Of course, this would not necessarily be true for operating modes in a monopole layout between one half boom and the S/C.

[14] Once the geometrical model has been built, the problem reduces to solving a linear set of equations where the number of unknowns consists of all pulsating charges corresponding to the total number of finite elements, i.e., N_q, plus the voltages of all conducting parts, i.e., N_v. Each set of equations is defined as follows.

[15] 1. For each finite element with subscript i, located on the part with subscript j, the induced voltage V_j is given by

$$V_j = V_{ii} + \sum_{k=1,\neq i}^{N_q} \frac{q_k}{4\pi\varepsilon_0 r_{ik}} \frac{\phi}{\phi_0}\left(\Omega, \frac{r_{ik}}{\lambda_D}\right) - E_l\, r_i, \qquad (3)$$

where V_{ii} is the voltage induced on the element in question by its own charge distribution; q_k is the complex pulsating charge $q_k \exp(i\omega t)$ carried by each element with the subscript k (assumed to be seen by all the others as located at its own geometrical center); r_{ik} is the distance from element i to k; ϕ/ϕ_0 is the plasma transfer function for a point source as defined by *Béghin* [1995], which depends on the frequency normalized with respect to the plasma frequency ($\Omega = \omega/\omega_p$) and on the distance normalized with respect to the Debye length; E_l is the longitudinal component of a possible external electric field; and r_i is the longitudinal coordinate of the element with respect to an arbitrary point of reference, defined as being at plasma potential. This point is taken at the center of the S/C body since all voltages are referred to the body. The value of V_{ii} is obtained assuming a uniform charge distribution on the surface of the element concerned, i.e.,

$$V_{ii} = \frac{q_i}{4\pi\varepsilon_0 S_i} \iint_{s_i} \frac{\phi}{\phi_0}\left(\Omega, \frac{|r|}{\lambda_d}\right) \frac{dS}{|r|} \equiv \alpha_S \frac{q_i}{4\pi\varepsilon_0 \Delta r}, \qquad (4)$$

where Δr is the characteristic dimension of the element (e.g., the radius for a sphere) and the coefficient α_S is given by an analytic expression derived from the above integral. Notice that while we assume a uniform charge distribution on each individual element, its own edge effect is not taken into account explicitly, though this effect will appear globally with charges accumulated on the terminal elements of the relevant part. This supposition holds also for a spherical element since its charge distribution remains globally uniform whenever the contact area with the closest element is small compared to the sphere itself. Nevertheless, a small correction is introduced in the code in order to account for the finite size of the elements compared to the Debye length. Using the first terms for the expansion of the function ϕ/ϕ_0 [*Béghin*, 1995], we get, for instance, the following value of α_S for a sphere of radius a:

$$\begin{aligned} \mathrm{Re}(\alpha) &= 1 + \frac{2}{\pi}\left(\frac{a}{\lambda_D}\right)\mathrm{Re}L_0 + \frac{1}{2}\left(\frac{a}{\lambda_D}\right)^2 + 0\left(\frac{a}{\lambda_D}\right)^3 \\ \mathrm{Im}(\alpha) &= \frac{2}{\pi}\left(\frac{a}{\lambda_D}\right)\mathrm{Im}L_0 + 0\left(\frac{a}{\lambda_D}\right)^3, \end{aligned} \qquad (5)$$

where L_0 is given by

$$\begin{aligned} \mathrm{Re}L_0 &= 0 && \Omega \geq 1 \\ \mathrm{Re}L_0 &= -\frac{\pi\Omega}{2\sqrt{3}\sqrt{1-\Omega^2}} && \Omega < 1 \\ \mathrm{Im}L_0 &= \frac{1}{\Omega}\sqrt{\frac{\pi}{2}}\left(\frac{\Omega^2}{\Omega^2-1}\right)^{\beta} && \Omega > 1 \qquad (\beta \approx 0.4348) \\ \mathrm{Im}L_0 &= \frac{\Omega}{2}\sqrt{\frac{\pi}{2}} && \Omega \leq 1. \end{aligned} \qquad (6)$$

[16] 2. For each individual part of the device except the central S/C body, its own voltage referred to this body is given by a specific electrical interface equation, such as

$$V_j - V_{\mathrm{S/C}} = i\omega Z_j \sum_{S_j} q_i + V_{0j}, \qquad (7)$$

where V_{0j} is the voltage (if any) applied to the part with the subscript j, Z_j is either zero or the impedance through which the current returns to the S/C, and the sum is taken over the individual charges on all the elements used in modeling the entire surface S_j of the part considered.

[17] A special case applies to the receiving probe, which is made of a sphere and a thin wire. In this case, equation (7) is replaced by a set of two; one of them is the same as (7) for the thin wire, where the sum of the charges involves both parts, and the second one is for the sphere, i.e., simply $V_{\mathrm{sphere}} = V_{\mathrm{wire}}$. Here Z_j is the high-input impedance of the preamplifier Z_{in} which is difficult to measure accurately in a laboratory. We have taken the most likely value, which is a capacitance of 4 or 5 pF shunted by a large resistance of at least 100 MΩ (L. Ahlen, private communication, 2003).

[18] 3. The final equation expresses the condition of charge neutrality for the entire system,

$$\sum_{i=1}^{N_q} q_i = 0. \qquad (8)$$

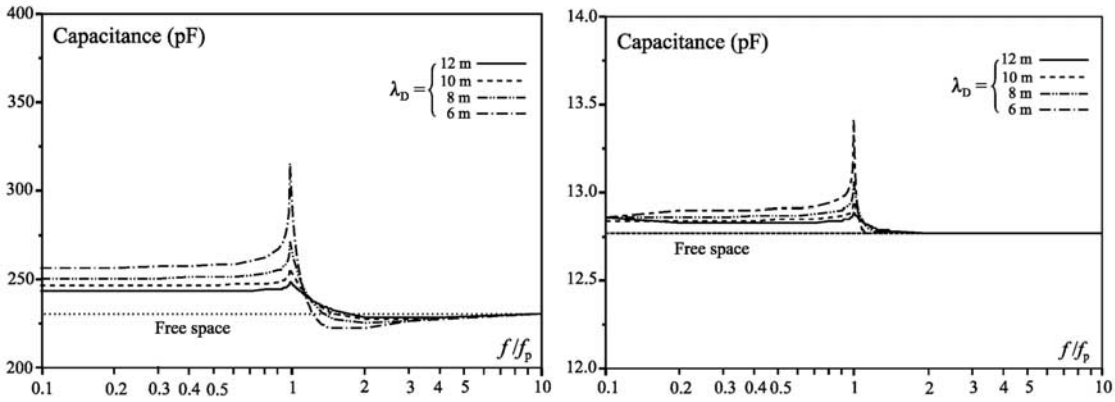

Figure 3. Capacitance of each monopole (left) of the wire boom and (right) of the double-probe antennas versus the frequency normalized with respect to the plasma frequency, as a function of the Debye length.

This linear system is closed, and the computation consists of inverting the $(N_q + N_v)$-dimensional complex matrix. The only difficulty for the code developer is to optimize the accuracy and the efficiency for a large number of elements which can be as much as several thousand in some instances [*Geiswiller et al.*, 2001].

4. Results of the Simulation

[19] We now summarize the main results of our simulations, in free space and space plasma, concerning (1) the self-impedances of both the double-wire and the double-probe antennas, (2) the mutual coupling between them under the conditions of the actual flight test, and (3) the effective length of the double-probe antenna.

4.1. Self-Impedances

[20] The self-impedance of the double-wire dipole is obtained assuming each monopole to be connected to a signal generator that feeds the dipole with a differential voltage balanced with respect to the S/C ground. The same is done for the impedance of the double-probe dipole. The amplitude of the current drawn by the antenna and its phase with respect to the voltage yields the complex impedance in terms of a reactance with a resistance in series. In the range of Debye lengths considered (6–12 m), the reactance is expected to be capacitive even near the plasma resonance, and the resistance is expected to be only the thermal wave radiation resistance because EM radiation is negligible in the frequency range considered. These assumptions are confirmed by the code results, as briefly reported below.

[21] The free space capacitances of the two antennas, with respect to infinity, are easy to estimate analytically using the classical equations for a long wire and for a sphere:

$$C_{\text{wire}} = \frac{2\pi\varepsilon_0 l}{\ln l/r};\ C_{\text{sphere}} = 4\pi\varepsilon_0 a, \tag{9}$$

where l is the wire length, while r and a are the radii of the wire and of the sphere, respectively.

[22] From (9) the capacitance of each of the 40 m wire boom monopoles would be 212 pF, and that of the thin wire plus the sphere would be 13 pF. The values obtained by the code, i.e., 234 and 12.77 pF, respectively (Figure 3), are consistent with these estimates, given that the presence of the S/C structure is believed to increase the boom capacitance slightly.

[23] For frequencies lower than the plasma frequency the capacitance tends asymptotically toward a larger value than in free space, in agreement with the following analytic evaluation. Assuming a uniform charge distribution along the antenna, as is almost the case for the range of Debye lengths considered, the expression for the capacitance of a long wire can be obtained from

$$C_{\text{wire}} = \frac{Q}{V_0};\ V_0 \approx \frac{Q}{2\pi\varepsilon_0 l}\int_{\delta l}^{l/2} \frac{\phi}{\phi_0}\left(\Omega, \frac{x}{\lambda_D}\right)\frac{dx}{x}. \tag{10}$$

Here the contribution to the voltage V_0 at the center of the wire, according to an expression similar to (4) and to usual approximations, is assumed to come essentially from charges laying on two symmetrical portions around this position beyond a distance δl which is of the order of the wire radius or so. One can check that in free space where $\phi/\phi_0 = 1$, one gets the same value for C_{wire} as is obtained in (9) by setting $\delta l = r/2$ in (10). Obviously, we can keep the same value for δl in the case with plasma

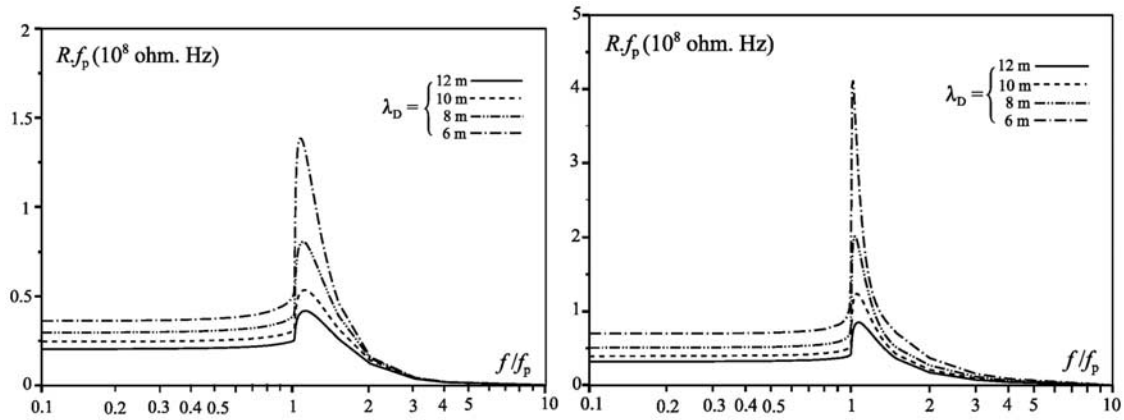

Figure 4. Resistance in ohm Hz units (see text) of each monopole (left) of the wire boom and (right) of the double-probe antennas.

whenever this distance is much shorter than the Debye length; then the change will come only from the behavior of the function ϕ/ϕ_0. At frequencies approaching zero the real part of this function tends to exp $(-x/\lambda_D)$ [*Béghin and Kolesnikova*, 1998], so the wire capacitance given by (10) becomes

$$C_{\text{wire}} \approx \frac{2\pi\varepsilon_0 l}{E_1\left(\frac{r}{2\lambda_D}\right) - E_1\left(\frac{l}{2\lambda_D}\right)} \quad (\Omega \ll 1), \qquad (11)$$

where E_1 is the exponential integral of the first order.

[24] When λ_D tends to infinity, we recover the free space value as given by (9), but for any finite Debye length the denominator in (11) is smaller than ln (l/r), so the low-frequency capacitance is greater than its free space value, in agreement with the code results plotted in Figure 3. Moreover, since the contribution of charges at large distances becomes negligible because of the second exponential integral in (11), the influence of the S/C body is less than in free space. This fact is confirmed by the code outputs, which fit the analytic expression (11) extremely well. For instance, for $\lambda_D = 10$ m the capacitance of a single wire boom is 250 pF as given by (11), while the code gives 242 pF for the low-frequency asymptotic value. Close to the resonance, antenna impedances are much more difficult to estimate analytically, and though this could be done, it is beyond the scope of this paper. At frequencies well above the resonance the capacitance obviously tends to its free space value, as is shown also in Figure 3.

[25] Now, in series with the capacitance that is the dominant part of the HF antenna impedance, there is a small displacement resistance, which must be not confused with the low-frequency Langmuir resistance. The latter is due to a conduction current in parallel with the HF impedance, while the series displacement resistance is due to the thermal waves that are radiated when the conducting surface reacts to the presence of electrons nearby. In the equations this resistance corresponds to the imaginary part of the plasma dielectric function ϕ/ϕ_0, the analytic expression for which is quite complicated [*Béghin*, 1995]. However, this expression can be simplified at frequencies below the plasma frequency, reducing to the so-called "screen function" which involves a limited volume within a few Debye lengths of the source [*Béghin and Kolesnikova*, 1998]. The low-frequency imaginary part of ϕ/ϕ_0 is given by

$$\text{Im}(\phi/\phi_0) \approx \frac{\Omega\rho}{\sqrt{2\pi}} F_s(\rho); \quad (\Omega \ll 1)$$

$$F_s(\rho) = \sum_{q=0}^{\infty} \{1 + 2q[\ln \rho - \psi(2q+2)]\} \frac{\rho^{2q}}{(2q+1)!},$$

$$\psi(n) = -\gamma + \sum_{k-1}^{n-1} \frac{1}{k}, \qquad (12)$$

where ρ is the normalized distance x/λ_D.

[26] By inserting (12) into an integral similar to (10) we can estimate the antenna resistance, again assuming a uniform charge distribution with a total charge mainly determined by the capacitance. In the case of an object smaller than λ_D, such as a small sphere, if we neglect the influence of any other conductor far away from it, we can use the first-order development of (12), which leads immediately to

$$R_0 = \frac{1}{4\pi\varepsilon_0\omega_P\lambda_D\sqrt{2\pi}} = \frac{0.92 \times 10^6}{\sqrt{T_e}}\,\text{ohm}; \qquad (\Omega \ll 1) \qquad (13)$$

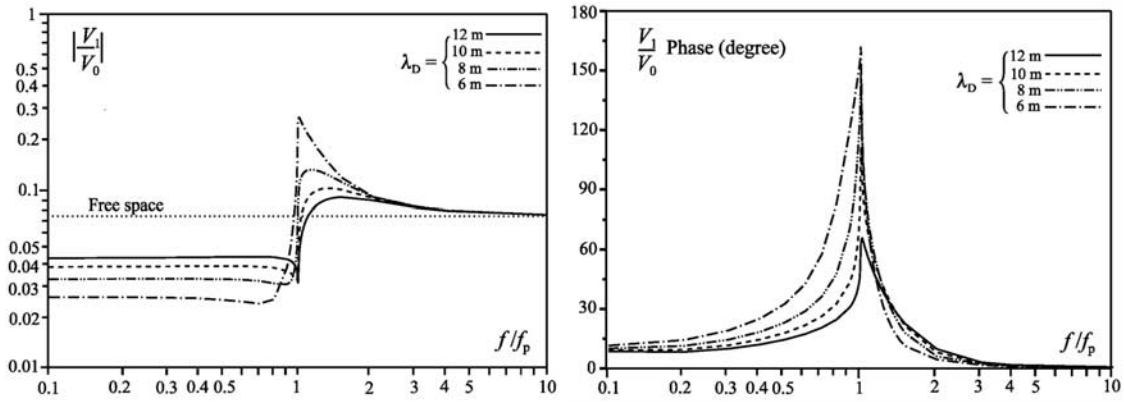

Figure 5. (left) Amplitude and (right) phase of the normalized mutual impedance between the wire boom and double-probe dipoles, defined as the ratio between the induced HF voltage on each probe (V_1) and the voltage applied to its associated wire boom (V_0).

where the unit for T_e is kelvin (K). Expression (13) is identical to that obtained by *Meyer-Vernet and Perche* [1989], who also considered a Maxwellian plasma but used a different approach aimed at estimating the thermal noise generated by such a resistance. For an ideal double-probe antenna with a tip-to-tip length much larger than λ_D, the low-frequency resistance of the dipole would be twice the individual value given by (13). For a double-wire dipole the analytic estimate is slightly more complicated, but it predicts that the resistance at the low-frequency plateau should be about half of that of a double-probe antenna with the same tip-to-tip length whenever this length ranges around about 6–12 λ_D.

[27] The results obtained with our code are plotted in Figure 4. For more generality, the values of resistance are given as the product Rf_p, which should be independent of f_p and depend only on λ_D. From (13) we get $Rf_p = 5.7 \times 10^8/\lambda_D$; hence the plateau values for each monopole of a double-probe antenna should vary from 0.475×10^8 up to 0.95×10^8 ohm Hz in the range of Debye length considered. The values obtained by the code (Figure 4, right) exhibit the expected behavior with the right order of magnitude, but they are ~30–40% smaller than the analytic estimate above.

[28] Just above the plasma frequency the antenna resistance exhibits a clear resonance which becomes sharper as λ_D decreases, as was expected theoretically and has been observed in space experiments, both by active measurements of impedance and by passive measurements of the spectrum of natural thermal noise [e.g., *Meyer and Vernet*, 1975; *Maksimovic et al.*, 1995].

4.2. Mutual Impedance

[29] The measurement of the mutual impedance is simulated by computing the signal induced on the double-probe when the wire boom dipole is fed exactly as for the self-impedance measurement. Thus both measurements are closely associated in the same procedure, as could be done experimentally. The amplitude and phase obtained by the code are plotted in Figure 5. In order to understand these results, we proceed as above with an analytic estimation of the frequency response below f_p. Again, we assume a uniform charge distribution along each monopole of the wire boom antenna, driven by the HF voltage V_0, which is here half the voltage feeding the dipole, so the induced voltage at the electric center of one of the receiving probes is

$$V_1 = \frac{C_{\text{wire}} V_0}{4\pi\varepsilon_0 l}\left[\int_{d_1}^{d_1+l} \frac{\phi}{\phi_0}\left(\Omega, \frac{x}{\lambda_D}\right)\frac{dx}{x} - \int_{d_2}^{d_2+l} \frac{\phi}{\phi_0}\left(\Omega, \frac{x}{\lambda_D}\right)\frac{dx}{x}\right], \quad (14)$$

where d_1 is the distance (~2.5 m) between the tip of the active shield of the wire boom and the electric center of the receiving probe, this center being on the thin wire at an estimated distance of ~0.9 m outward from the puck (Figure 2); l is the length of the active shield on each monopole (~40 m); and d_2 is the distance between the feed point of the opposite active shield and the electric center of the receiving probe (~45.5 m). Here, for simplicity, we will use a constant value $C_{\text{wire}} = 234$ pF for both the free space and the plasma conditions. As a rough approximation, we assume that the entire receiving probe is floating at the voltage given by (14) for a single point. Then we get the following free space response:

$$\frac{V_1}{V_0} = \frac{C_{\text{wire}}}{4\pi\varepsilon_0 l}\ln\left[\frac{d_2(d_1+l)}{d_1(d_2+l)}\right] = 0.116. \quad (15)$$

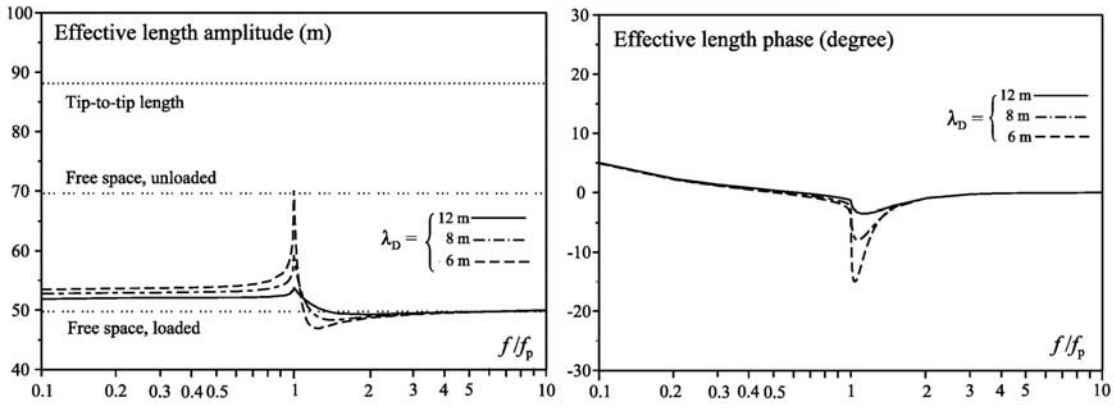

Figure 6. (left) Amplitude and (right) phase variations of the effective length of the double-probe dipole as a function of the frequency for different Debye lengths.

Moreover, the probe is loaded by the input capacitance of the preamplifier ($C_{in} \sim 4$ pF). Therefore the dynamic response will be reduced through the action of the capacitance divider formed by C_{probe} and C_{in} in series. With $C_{\text{probe}} = 12.8$ pF the free space response becomes $V_1/V_0 = 0.088$, while the code (Figure 5, left) gives a value quite close to this (0.074).

[30] In the plasma at low frequency, using the above asymptotic expression $\phi/\phi_0 = \exp(-x/\lambda_D)$, we get from (14)

$$\frac{V_1}{V_0} = \frac{C_{\text{wire}}}{4\pi\varepsilon_0 l}\left[E_1\left(\frac{d_1}{\lambda_D}\right) - E_1\left(\frac{d_1+l}{\lambda_D}\right) - E_1\left(\frac{d_2}{\lambda_D}\right) + E_1\left(\frac{d_2+l}{\lambda_D}\right)\right], \tag{16}$$

which is significantly different from (15) because of the behavior of the exponential integral function. The result is to decrease the mutual impedance by a factor of ~2. For instance, for $\lambda_D = 8$ m we find from (16) that $|V_1/V_0| \sim 0.04$ when the probe is floating and 0.03 when it is loaded by C_{in}. The value given by the code ($|V_1/V_0| = 0.032$), as seen in Figure 5 (left), is very close to this estimate.

[31] Another remarkable feature revealed by the code is the pronounced minimum of $|V_1/V_0|$ just below the plasma frequency, which appears for a particular range of Debye lengths (e.g., $\lambda_D = 10-12$ m, in Figure 5 (left)). This feature can also be predicted by a simple analytic estimation, using the asymptotic approximation for ϕ/ϕ_0 at the plasma frequency [*Béghin and Kolesnikova*,1998], which is

$$\frac{\phi}{\phi_0}(\Omega = 1) \approx 1 + \frac{x^2}{6\lambda_D^2}. \tag{17}$$

This states that the HF electric potential ϕ created by a single point charge is the sum of the free space potential which decreases as $1/x$ with increasing distance, plus a term that actually increases with increasing distance in direct proportion to x; this second term is inversely proportional to λ_D^2. Hence the potential induced at the surface of the receiving antenna results essentially from the nearest portion of the emitting antenna for the free space contribution and from the farthest portion for the plasma contribution. Since the dipole is fed symmetrically with a differential HF voltage, these two contributions have opposite phases, and it is their mutual cancellation that produces the observed minimum in the mutual impedance when the conditions are such that their amplitudes are more or less equal.

[32] This effect may be estimated by putting the expression (17) into (14), leading to

$$\frac{V_1}{V_0} = \frac{C_{\text{wire}}}{4\pi\varepsilon_0 l}\left[\ln\left(\frac{l+d_1}{d_1}\frac{d_2}{l+d_2}\right) - \frac{l(d_2-d_1)}{6\lambda_D^2}\right], \ (\Omega = 1), \tag{18}$$

which gives the mutual impedance at the plasma frequency with the same assumption as above, that is, that each receiving probe takes the voltage at its electric center. Then we get

$$\left(\frac{V_1}{V_0}\right)_{\Omega=1} = \left(\frac{V_1}{V_0}\right)_{\text{free space}}\left[1 - \left(\frac{11.4}{\lambda_D}\right)^2\right]. \tag{19}$$

This approximation predicts that the amplitude would be strictly zero when $\lambda_D = 11.4$ m. However, we have neglected the contribution of the imaginary part in (17), which is significant at short distances [*Béghin*, 1995]. Nevertheless, since the imaginary part is small, the

amplitude can reach a sharp minimum at the plasma frequency. This surprising prediction has been confirmed by the flight test results, which are presented in section 5. When λ_D increases well above this particular value, we see from (18) and (19) that the response tends to the free space value while the minimum is becoming shallower progressively, which is confirmed by the code (not shown in Figure 5).

4.3. Effective Length of the Double-Probe Antenna

[33] The amplitude and phase of the effective length of the Cluster double-probe antenna, as defined in the ways described in section 2 and as obtained by the code, are plotted in Figure 6. The first comment is that even in free space and on open circuit, i.e., with Z_{in} infinite in (1), the effective length l_{ef} is distinctly less than the conventional tip-to-tip length l, as is shown in Figure 1: The effect of the grounded outer shield of the long boom reduces l_{ef} from 88 m down to 69 m. When the probe is loaded by the input impedance of the preamplifier (5 pF, 10^8 ohm in the case of Figure 6), the acting effective length is reduced further, according to (1) and (2), by the ratio $C_{\text{probe}}/(C_{\text{probe}} + C_{in})$, bringing it down to ~50 m. This is exactly what we get from the code (Figure 6, left).

[34] For the antenna in the plasma, Figure 6 shows only the acting effective length, which is the parameter deemed most useful for interpreting natural wave measurements. As expected, above about twice the plasma frequency the effective length is almost equal to that in free space in both amplitude and phase over the entire range of Debye lengths. At lower frequencies we observe a plateau for the amplitude, which lies between ~52 and 53 m and depends slightly on λ_D, while the phase exhibits a small shift that increases with decreasing frequency and is due to the resistive part of the preamplifier input impedance.

[35] Close to the plasma frequency the effective length exhibits the effect of the antenna resonance more and more strongly as the Debye length decreases. This behavior must be fully taken into account when interpreting the measured level of natural quasi-static emissions, of the Langmuir type for instance. It is very important to realize that the behavior we see here is typical of any double-probe antenna: its effective length is strongly influenced by the guards (i.e., the grounded outer shields of the cables), especially in the vicinity of the resonance [*Béghin*, 2002]. The situation is more favorable with an ordinary double-wire dipole because (1) its self-impedance is usually much smaller than the load impedance and (2) the electric center of each monopole lies near to the geometric center, more or less independently of the plasma conditions so long as the effective length is not greater than about 10–15 Debye lengths. For that reason it would be unwise to compare double-probe and double-wire dipole measurements without a careful analysis of the above considerations.

5. Flight Test Results

[36] The wave measurement system installed on Cluster was not designed for measuring the mutual coupling between the wire boom and double-probe dipoles. Nevertheless, by taking advantage of the flexibility of the system we ran an unusual mode of joint operation involving the relaxation sounder WHISPER [*Décréau et al.*, 1997] and the waveform receiver WBD [*Gurnett et al.*, 1997]. This was done with the wire boom dipole used as the emitting antenna of the sounder and the associated double-probe dipole used as the receiving antenna. Unfortunately, among several hardware constraints which were unsatisfactory for making such a measurement, the main one was the high level of the signal applied by WHISPER to the emitting dipole, which could not be reduced below 50 V (peak amplitude of sine wave). According to our simulation this strong signal would have induced ~3.6 V at the receiver input in free space conditions. Disregarding possible nonlinear effects in the surrounding plasma, this level corresponds nearly to the nominal upper limit of the dynamic range for the WBD receiver above which saturation and clipping occur. Therefore we will present here a preliminary interpretation of the results, using only data that lay marginally inside the normal linear range of the instrument; only the amplitude of the mutual impedance response, without the phase, could be derived in this preliminary investigation.

[37] For precise comparison between the theoretical modeling and the flight data, if such a mode of operation had been planned originally, the ideal procedure would have been to calibrate the entire loop transfer function of the WHISPER-WBD hardware alone (independently from the external medium) during the ground operations and to make similar calibrations periodically in orbit. For lack of that, we have had to construct a dedicated calibration function, which contains several factors of uncertainty.

[38] Before we present the results and comment on the confidence levels we show the calibration data, which after a careful investigation have been used for this unusual mode of operation. The normalized mutual impedance response, as defined in section 4.2, is the ratio of the received signal V_r to the emitted signal V_e, and it is expressed here by

$$\frac{V_r}{V_e} = \frac{N}{V_e} \frac{\gamma}{\alpha \beta}, \tag{20}$$

where N is the 8-bit peak-to-peak raw amplitude (0–255) of the waveform measured in the WBD data files for a

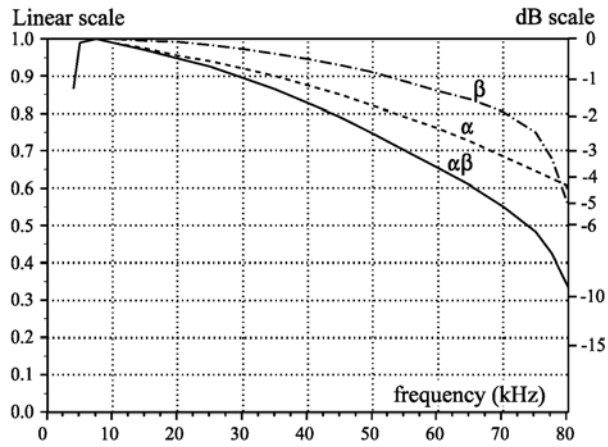

Figure 7. Calibration curves for the mutual impedance mode between WHISPER and WBD. Note that α is the transfer function of the transmitter normalized to the nominal amplitude of 50 V applied to the wire boom dipole (H. Seran, private communication, May 2004) and β is the WBD normalized frequency response in the 77 kHz bandwidth.

given frequency step of the WHISPER emission; α and β are the normalized transfer functions versus frequency of the transmitter and of the receiver, respectively, in both linear and dB scales (Figure 7); γ is the 0 dB hardware transfer function of the receiver, defined as a ratio between the amplitude of the HF voltage received on the double-probe antenna and the corresponding 8-bit peak-to-peak output count; and V_e is the 0 dB nominal amplitude of the voltage fed to the transmitting dipole (50 V). In the absence of in-flight calibration we take the conventional value of γ, which corresponds to an electric field of amplitude 36.9 mV m^{-1}, the largest amplitude that can be measured by the WBD in the 77 kHz bandwidth mode without clipping. This field was calculated by assuming arbitrarily an effective antenna length of 88 m, leading to $\gamma = 36.9 \times 10^{-3}$ (88/255) = 1.273 10^{-2} V per count unit.

[39] We emphasize that precise calibration is needed for this experiment; it requires an absolute accuracy of 1 dB or even better for fitting the experimental data to the theoretical curves produced by the modeling. Considering the quality and the reproducibility of the raw data during our flight test, which always appeared as pure sine waves, we find no evidence for any nonlinear effects in the surrounding plasma. We think that the above level of accuracy was achieved for the data shown hereafter, except where otherwise stated, as, for instance, for some short portions of clipped signals.

[40] The test was performed on board SC 1 (Rumba) on two occasions in sequences of 15 mn duration each. The first test was made on 11 April 2004 between 0045 and 0100 UT in the magnetosheath region (L = 12.70, magnetic local time (MLT) is 0964), and the second was made on 14 May 2004 between 2210 and 2225 UT in the preshock solar wind region (L = 33.15, MLT = 0820). Typical samples of the mutual impedance response are plotted in Figure 8 together with the theoretical model curves that fit the data best. At a first glance, the Maxwellian model seems to fit the observed responses very well for frequencies around and above the plasma frequency ($\Omega = 1$). During the time interval (0045:30–0047:30 UT), corresponding to the sample plotted in Figure 8 (left), the plasma resonance seen simultaneously by WHISPER (in the sounder mode on the double-probe antenna perpendicular to the one used for our tests) and by WBD (on the one that we used), ranged ~44–45 kHz, i.e., n_e = 24–25 cm^{-3}. For the sample from the second pass (2210:30–2211:12 UT), corresponding to the plot in Figure 8 (right), these values were 36.75–37.75 kHz and 16.7–17.6 cm^{-3}, respectively.

[41] As predicted by the model, we see in both cases a clear minimum just below $\Omega = 1$, and an apparent value of the Debye length might be deduced from the fit with the model above that frequency. One can retain $\lambda_D \sim$ 11 m for the first pass and 10 m for the second one. From the well-known relationship between the electron temperature, the Debye length, and the plasma frequency, which is

$$T_e = 2.6 \times 10^{-6} \left(f_p \lambda_D\right)^2 \qquad (21)$$

in the SI unit system, and knowing that 1 eV = 11500 K, we deduce from the above values an electron temperature of about 6.2×10^5 K (i.e., 54 eV) for the first pass and 3.6×10^5 K (i.e., 31 eV) for the second one. Such high temperatures seem quite unusual in these regions, especially a value above 30 eV in the preshock solar wind region. Moreover, the low-frequency response ($\Omega <$ 0.8) does not fit this model at all; to make it fit, the Debye length would have to be much larger than 10 m, leading to correspondingly greater temperatures. In addition, the two samples exhibit quite different shapes around the minimum, whereas the apparent Debye lengths inferred from the HF response are quite similar. The first possible cause of discrepancy with respect to our model could be that the condition of plasma isotropy is not satisfied. Nevertheless, this does not seem to be the case because of the absence of a significant spin modulation in the mutual impedance response. The measured average amplitude of the steady magnetic field lies around 28.5 nT in the first region and 8 nT in the second one. These values correspond to a ratio of the cyclotron frequency to the plasma frequency of about 2×10^{-2} and 5×10^{-3}, respectively, which is too small to account for the observed discrepancy.

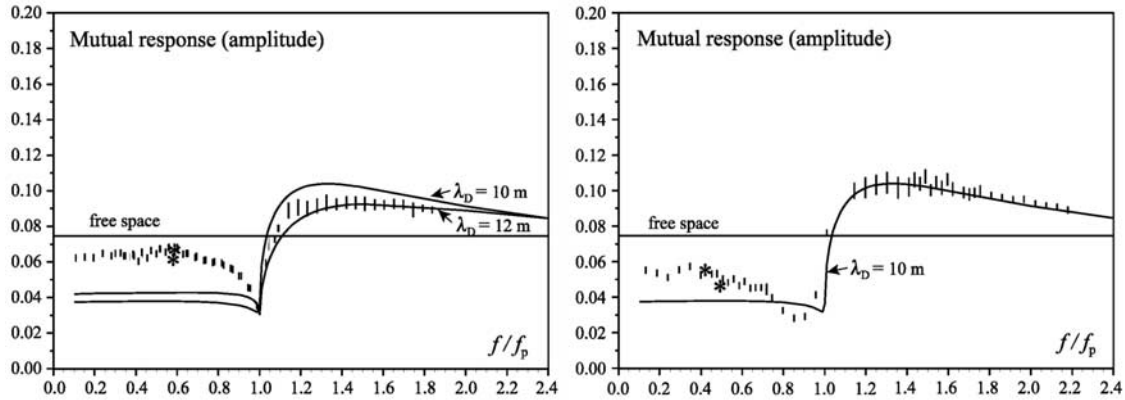

Figure 8. Samples of experimental response (error bar plots) of the mutual impedance WHISPER/WBD measured (left) on 11 April 2004 in the magnetosheath and (right) on 14 May 2004 in the preshock solar wind region. Data are plotted together with the theoretical responses given by both the Maxwellian model (solid lines) and the two-component model at $\Omega_h = 1$ (asterisks), with $\mu = 0.5$, $\tau = 2$ (top asterisk), and $\tau = 4$ (bottom asterisk) for the first pass and with $\tau = 9$, $\mu = 0.2$ (top asterisk), and $\mu = 0.3$ (bottom asterisk) for the second pass.

[42] After having ruled out all possible hardware or calibration artefacts that could produce such an effect, we concluded that a simple Maxwellian distribution would not suffice to account for the observations. Since the present version of our code does not provide for a non-Maxwellian distribution, we have developed in the meantime an analytic approximation assuming an electron distribution with two Maxwellian components: one cold, which is the major one, and the other hot. A similar analytic approach has been proposed in case of thermal noise induced by different kinds of non-Maxwellian plasmas [*Chateau and Meyer-Vernet*, 1991]; however, since their study is applicable to the real part only of the impedances, we will proceed with a different way. Here a two-population distribution enables us to account satisfactorily for the observations, at least to a first order as presented below.

[43] In order to derive the function ϕ/ϕ_0 in the case of a two-component distribution we must introduce two new parameters. They are $\mu = n_h/n_c$, the ratio between the hot and cold electron densities, and $\tau = T_h/T_c$, the ratio between the hot and cold temperatures. The global plasma frequency is still f_p, while λ_{Dc} is now the Debye length of the cold population, which we will take here as a reference. From these we define the following normalized parameters which will be used hereafter:

$$\Omega = \frac{f}{f_p};\ \Omega_c = \frac{f}{f_c}\Omega\sqrt{1+\mu};\ \Omega_h = \Omega\sqrt{\frac{1+\mu}{\mu}};$$
$$\lambda_{Dh} = \lambda_{Dc}\sqrt{\frac{\tau}{\mu}};\ (\mu < 1;\ \tau > 1), \tag{22}$$

where f_c and f_h are the plasma frequencies of the cold and hot populations, respectively. Starting from the basic equations given by *Béghin* [1995], the function ϕ/ϕ_0 for a pulsating point source is again given by

$$\frac{\phi}{\phi_0} = \frac{2}{\pi}\lim_{\mathrm{Im}\,\omega \Rightarrow 0}\int_{-\infty}^{0}\frac{\sin kr}{kr}\frac{dk}{\varepsilon_l(k,\omega)}, \tag{23}$$

where ε_o is the free space permittivity, k is the wavenumber, $\varepsilon_l\ (k, \omega)$ is the longitudinal dielectric permittivity, and $\omega = 2\pi f$ is the complex frequency, bearing in mind that $\varepsilon_l\ (k, \omega)$ is the limit reached when the small negative imaginary part of ω tends to zero, corresponding to the steady state of the source after a transient growing phase. In the quasi-static approximation, the dispersion equation is $\varepsilon_l\ (k, \omega) = 0$ which reads here

$$\varepsilon_l(k,\omega) = 1 - \frac{z_c^2}{\Omega_c^2}Z'(z_c) - \frac{z_h^2}{\Omega_h^2}Z'(z_h) = 0, \tag{24}$$

where Z' is the first derivative of the dispersion function $Z(z)$ for a Maxwellian plasma [*Fried and Conte*, 1961], the definition of which is

$$Z(z) = \frac{1}{\sqrt{\pi}}\int_{-\infty}^{\infty}\frac{e^{-x^2}}{x-z}dx \quad (\mathrm{Im}\,z > 0) \tag{25}$$

with an analytic continuation for Im $z \leq 0$; the variable quantity z is the ratio between the wave phase velocity

and the thermal velocity of the relevant distribution. Hence, using the other parameters defined in (22), we get

$$z_c = \frac{\Omega_c}{\sqrt{2}k\lambda_{Dc}};\ z_h = \frac{z_c}{\sqrt{\tau}}. \tag{26}$$

[44] In the following, we will consider z_c alone as the variable quantity for a given value of τ, since z_h is just proportional to it. The function $1/\varepsilon_l$ can be expanded in the form of an infinite Mittag-Leffler series, involving the principal parts at all of its poles z_n in the complex plane. From (24) we get $1/\varepsilon_l = 1$ for $z_c = 0$, so we can write the Mittag-Leffler series as

$$\frac{1}{\varepsilon_l(z_c)} = 1 + \sum_{|n|}^{\infty}\left(\frac{b_n}{z_n} + \frac{b_n}{z_c - z_n}\right);\ b_n = \frac{1}{\left(\frac{d\varepsilon_l}{dz}\right)_{z=z_n}}, \tag{27}$$

where b_n is the residue at the pole of order n, and the ratio b_n/z_n is known as the excitation coefficient of forced oscillations. As in the case of a single Maxwellian, there are three families of poles, namely, the purely imaginary poles, the usual Landau waves above f_p, and the high-order poles described in detail by *Derfler and Simonen* [1969]. These are usually plotted in the complex plane of k or of its normalized value $K = k\lambda_{Dc}$ rather than of z. The rigorous approach should consist of introducing the expression (27) in (23), which amounts to adding successively the contributions of (1) the free space term, (2) the dominant poles, and (3) the high-order poles.

[45] A brief analysis of the solutions of (24) is presented in Appendix A, where we give the analytic expression (A8) for the excitation coefficients. It is also shown that for frequencies in a range around the global plasma frequency the contribution of the main Landau waves reduces to the same value as for a single Maxwellian distribution, provided that we consider a "hybrid" Debye length as given by (A3). This remark applies above $\Omega \sim 1$ to the theoretical curves that are compared with the flight test results in Figure 8. In this instance, we have to consider the Debye lengths (10 and 11 m) as "hybrid" values, assuming that the distribution is not a single Maxwellian. A similar approximation applies to the evanescent waves at low frequencies. The problem then is to decide which values of the adjustable parameters μ and τ should be adopted in our two-component model. We will estimate these two parameters by trying to fit a part of the low-frequency response, which deviates significantly from the curve for the value of λ_D that yields the best fit with the response curve at higher frequencies.

[46] For this purpose, we will derive an expression for the mutual impedance at low frequency by using an analytic approximation similar to the so-called Landau wave approximation [e.g., *Chasseriaux et al.*, 1972]. In the single Maxwellian case this approximation appears to be quite satisfactory at large distance when compared to the exact solution [*Béghin*, 1995]. Here we will use instead a short-distance approximation which is more suited to our specific conditions. Then, we will compare these estimates with data from the Plasma Electron and Current Experiment (PEACE), which measures the three-dimensional velocity distribution of electrons in the energy range from 0.6 eV to 26 keV during one spin period of the spacecraft [*Johnstone et al.*, 1997].

[47] In the usual approximation one assumes that the induced potential at several Debye lengths from the source is the sum of two contributions, one from the main Landau poles and the other from the cold plasma term (i.e., $T_e \sim 0$). However, it has been proved in the case of a single Maxwellian distribution [*Béghin*, 1995] that the contribution of the infinite series of high-order poles at large values of z (representing waves with large phase velocities) is not negligible, contrary to what is generally believed. In reality, this contribution tends asymptotically at large distances to 25% of the actual cold plasma contribution, in which it becomes included implicitly. In these conditions the contribution of the cold plasma is still $1/\varepsilon_c$, which validates the above approximation. In the case of a two-component distribution, since we are changing essentially the tail of the distribution, it is easy to understand that the transition point in particle velocity space, where the cold and hot populations are equally dense, must play an important role in the contribution of the high-order poles. For two Maxwellian distributions, denoted by the subscript $i = 1$ or 2, both of which obey the Boltzmann law

$$f_i(v) = n_i\left[\frac{m_e}{2\pi\mathbf{K}T_i}\right]^{3/2}\exp\left[-\frac{m_e v^2}{2\mathbf{K}T_i}\right], \tag{28}$$

the transition point occurs for a kinetic energy given by

$$\frac{1}{2}m_e v^2 = \frac{\mathbf{K}T_c \ln\zeta}{1-\tau^{-1}},\ \zeta = \frac{\tau^{3/2}}{\mu}, \tag{29}$$

where $\mathbf{K}$ is the Boltzmann's constant and $\ln\zeta$ is a parameter that governs the series of high-order poles (see Appendix A). Thus the change observed at low frequencies in the mutual impedance response is expected to come essentially from the contribution of these high-order poles ($K_{|n|>3}$). As long as we consider a frequency much smaller than the global plasma frequency, as for instance the plasma frequency of the hot population, and distances much shorter than the wavelength of these waves, it is shown in Appendix A that their global contribution may simply be estimated from the sum of their excitation coefficients defined in (27). In these conditions the modified Landau wave approximation for short distances leads to a quite simple

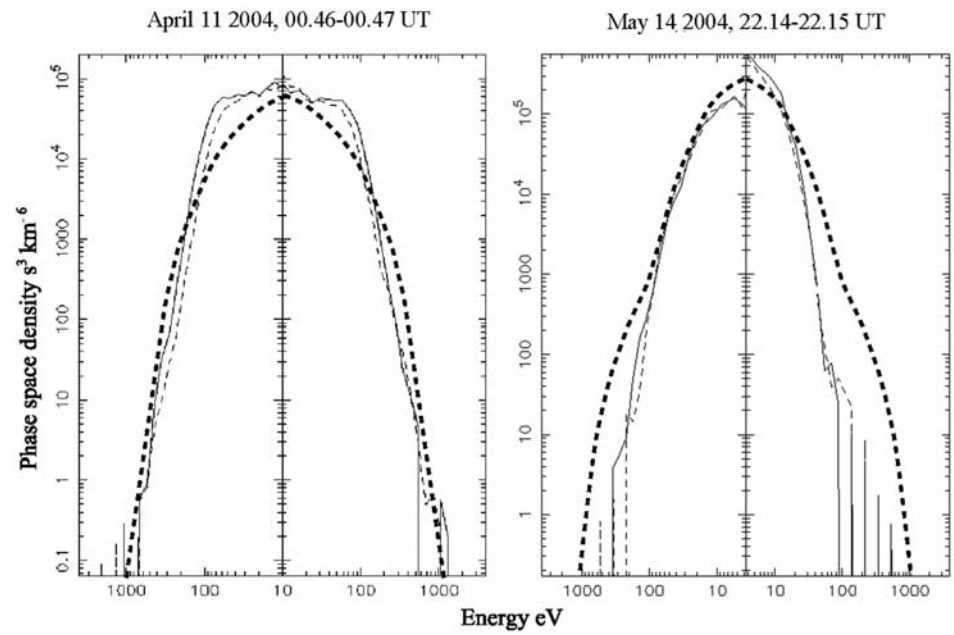

Figure 9. Cuts of the electron distribution function in the parallel and antiparallel directions as measured by the PEACE experiment during the two sample tests of mutual impedance. The solid and thin dashed lines correspond to data taken at ~1 min intervals, and the thick dashed line is the two-component distribution derived from the analytic model.

expression for ϕ/ϕ_0 given by (A14). The latter reduces simply to the free space term plus a contribution determined only by the evanescent poles. Finally, by using the same method as for (15) and (16) the analytic expression for the mutual impedance response becomes

$$\frac{V_1}{V_0} = \left[\frac{V_1}{V_0}\right]_f \left(1 + \sum_{-2}^{2} \frac{b_n}{z_n} - 2\frac{b_{-2}}{z_{-2}} \cdot \frac{E_1(d_1 k_{-2}) - E_1[(d_1 + l)k_{-2}] - E_1(d_2 k_{-2}) + E_1[(d_2 + l)k_{-2}]}{\ln\left[\frac{d_2(d_1 + l)}{d_1(d_2 + l)}\right]}\right) \tag{30}$$

where the subscript f refers to the free space response and k_{-2} is the wave number of the main imaginary pole z_{-2}. The procedure consists first of computing the two purely imaginary poles at $\Omega_h = 1$ from (24), then deducing their excitation coefficient from (A8) and the value of k_{-2} from (26).

[48] In this preliminary investigation we have considered the possible ranges of variation for the two parameters μ (from 0.1 to 1) and τ (from 2 to 10) in order to check if this simple model would allow us to explain the observations. The best fit obtained for each of the two passes is shown by the asterisks in Figure 8. It was expected that the plasma conditions would be different in the two regions where the tests were performed, but in fact, the "hybrid" Debye length (10–11 m) and the total electron density (24–18 cm^{-3}) are quite similar. Nevertheless, our estimate leads to $\tau \sim 2$ and $\mu \sim 0.5$ for the pass on 11 April (Figure 8, left) in the magnetosheath and to $\tau \sim 9$ and $\mu \sim 0.2$ for the pass on 14 May (Figure 8, right) in the preshock region. These values correspond to $n_c = 16$ cm^{-3}, $T_c \sim 39$ eV, $n_h = 8$ cm^{-3}, and $T_h \sim 79$ eV for the first pass, assuming $\lambda'_D = 11$ m and $n_c = 14$ cm^{-3}; and $T_c \sim 12$ eV, $n_h = 2.7$ cm^{-3}, and $T_h \sim 108$ eV for the second one with $\lambda'_D = 10$ m. As the two measurements were performed more than 1 month apart, it would be not worth our while to comment in more detail on to the geophysical meaning of such different distributions especially as this would be beyond the scope of this paper.

[49] The next step was to compare the above results with the measurements of the electron flux made by the experiment PEACE. The shape of the observed electron energy distribution is plotted in Figure 9 for the relevant time periods on each pass as a cut along the directions parallel and antiparallel to the magnetic field. In the magnetosheath the distribution is clearly of the flattop type, which is a common occurrence in that region [e.g., *Feldman et al.*, 1982]. The electron density, deduced as the zero-order moment of the distribution function using the Queen (Mary) Truncated Moments Corrector

(QTMC) code [*Génot and Schwartz*, 2004], is found to be about 24–25 cm^{-3}, with an average of 38–39 eV for the parallel and perpendicular temperatures. This value of the total density is the same as obtained from our active experiment, and the temperature is that of the major constituent derived from our two-component distribution model. In Figure 9 (left) we have plotted the combined, two-component distribution function alongside the PEACE data, and we judge the fit for this pass to be quite satisfactory.

[50] A similar comparison for the second pass (Figure 9, right) is less satisfactory. The best estimate of the zero-order moment from the PEACE data for this sample, using the actual value of the S/C potential (+2.9 to 3.9 V) obtained from the Electric Field and Wave experiment [*Gustafsson et al.*, 1997], leads to an average electron density of 13–15 cm^{-3}, which is the same as our estimate of the major component deduced from the mutual impedance measurement but slightly lower than the total density deduced from the plasma resonance. However, the shape of the distribution measured by PEACE, as plotted in Figure 9 (right), is significantly different from that of our analytic model. The PEACE's data could fit a two-component distribution representing a major constituent with an electron density of 13–15 cm^{-3} and a temperature of 6.5–8 eV, plus a weak suprathermal component with a density of $\sim$0.1 cm^{-3} and a temperature of 80 eV. Except for a good agreement on the density of the cold population with a more or less compatible temperature, it appears either that the density of the suprathermal component seen by PEACE has been underestimated or, more likely, that the one deduced from the mutual impedance has been overestimated.

[51] Indeed, because of the limitations of our analytic approximation we cannot rule out the possible importance of other secondary effects that have been neglected in this preliminary interpretation, for instance, the effect of bulk plasma drift in the S/C reference frame, which is significant in this case, with a velocity of $\sim$500 km s^{-1}. Other deviations from an isotropic distribution were seen by PEACE on this second pass: a temperature anisotropy of the order of 20% between the directions perpendicular and parallel to the steady magnetic field and an asymmetry of the distribution function in the plasma reference frame, which is the signature of a heat flux in the antiparallel direction. However, these last two deviations are believed to have only a minor effect on the mutual impedance response compared to the drift effect. On the other hand, in a tenuous plasma both experiments may be more sensitive to the nearly constant flow of photoelectrons emitted from and impacting the S/C body than they are in a dense plasma.

[52] Regardless of the respective constraints of each measurement which appeared clearly in this preliminary test, the complementarity of both experiments encourages us to pursue such comparative studies, specifically in order to improve our modeling of electric antennas in complex plasma conditions in view of geophysical applications.

6. Conclusion

[53] The aim of this paper was to present an exhaustive analysis of the present state of art for modeling of electric antennas in a kinetic space plasma. Though our method is based on restrictive hypotheses, it remains to date one of the most advanced approaches for modeling long electric antennas in space plasmas. Most of the physical mechanisms are well understood as a result of this study, and it now appears that the design of the Cluster antennas, which has evolved from long experience, is well suited to the plasma environment in the HF domain considered here. We believe that the main electric characteristics deduced from our model are applicable to the equivalent circuit of these antennas. We recommend in particular that our evaluation of the actual effective length, as plotted in Figure 6, should be used instead of the physical length whenever accurate values of amplitude and phase of HF electric field components are needed.

[54] The successful test in flight of the mutual impedance measurement, performed in April and May 2004, has globally validated our modeling. A first-order fit between observed and theoretical curves, obtained not only with the absolute amplitude but also with the shape, allows us indeed to deduce the electron density from the frequency of the plasma resonance and the average electron temperature from an apparent Debye length. However, the test has revealed one important limitation coming from our initial assumption of an isotropic Maxwellian electron distribution. Since the mutual impedance response does not exhibit any significant anisotropy, which would have been revealed by perturbations repeating with the spin period, we believe that the discrepancy between the observed low-frequency response and that of the basic model must be the signature of a non-Maxwellian distribution. This assumption is broadly confirmed by the data from the experiment PEACE, which provides the energy distribution of electrons impacting the detectors. A rough analytic approximation based on an equivalent two-component electron distribution allows us to account for the anomaly in the low-frequency response of the mutual impedance.

[55] This simple model allowed us to estimate the proportions of both components, though such estimates are found to be in better agreement with the PEACE data for the first pass than for the second one. We hope that further investigation considering additional secondary effects, such as those due to a bulk plasma drift, will

enable us to obtain better agreement between the plasma parameters derived from these different techniques. We must point out that since we have restricted our approximation to the response in a small range around the supposed plasma frequency of the minor component, we do not take advantage of all the information contained in the entire range of frequency. Therefore further development of the numerical code will necessarily include the full kinetic treatment for a non-Maxwellian distribution and/or for a drifting plasma in order to confirm the above speculations.

Appendix A

[56] Let us consider first the solution of (24) for the main Landau poles (z_1 and z_{-2}) around f_p, using here the same notation as by *Béghin* [1995]. For $\Omega \gtrsim 1$, we are expecting the poles to lie close to the real axis, such as $|z| \to \infty$, i.e., $|k| \to 0$, so we can use the following asymptotic development:

$$z^2 Z'(z) = 1 - 4iz^3\sqrt{\pi}e^{-z^2} + \frac{2}{2z^2} + \frac{15}{4z^4} + \ldots; \cdot (|z| \gg 1,\ \mathrm{Im}(z) < 0). \quad \text{(A1)}$$

As a first-order approximation, and assuming a low damping rate by neglecting the imaginary part in (A1), we get from (22) and (24)

$$\varepsilon_l \approx 1 - \frac{1}{\Omega^2} - \frac{3}{2z_c^2\Omega_c^2} - \frac{3\mu\tau}{2z_c^2\Omega_c^2};\ (\Omega \approx 1), \quad \text{(A2)}$$

which is the same as the conventional Landau dispersion equation, albeit involving a "hybrid" Debye length given by

$$\lambda_D' = \lambda_{Dc}\sqrt{\frac{1+\mu\tau}{1+\mu}};\ (\Omega \approx 1). \quad \text{(A3)}$$

[57] For frequencies just below f_p, as long as $|z| \gg 1$, equations (A2) and (A3) are still valid, but z_c^2 now takes a very large real negative value, leading to the usual evanescent pole z_{-2} corresponding to the wave number k_{-2}, which is nearly zero on the negative imaginary axis. However, at low frequencies when $\Omega \Rightarrow 0$, the modulus of z_{-2} decreases rapidly, so we can use the power series for Z', the first terms of which are

$$Z'(z) \approx -2 + 4z^2 - 2iz\sqrt{\pi}e^{-z^2};\ (|z| \ll 1). \quad \text{(A4)}$$

Then (24) becomes

$$\varepsilon_l \approx 1 + \frac{2z_c^2}{\Omega_c^2}\left[1 + \frac{\mu}{\tau}\right];\ (\Omega \Rightarrow 0), \quad \text{(A5)}$$

which is the same as the dispersion equation for the evanescent waves ($k_2\,\lambda_D = I$ and $k_{-2}\,\lambda_D = -i$) of a single Maxwellian distribution, provided that we introduce a new hybrid Debye length given in this case by

$$\lambda_D'' = \lambda_{Dc}\sqrt{\frac{\tau}{\tau+\mu}};\ (\Omega \Rightarrow 0). \quad \text{(A6)}$$

As long as we are considering $\mu/\tau \ll 1$, the above dispersion equation (A5) does not present any significant difference with respect to the case of a single Maxwellian. In the experimental conditions of the tests the very low frequency response of the mutual impedance mode was not observable below $\Omega \sim 0.2$, so we are not able to check the validity of the above asymptotic equations for $\Omega \to 0$. Accordingly, we will limit our analysis to a range of low frequencies around the plasma frequency of the minor constituent, i.e., $\Omega_h \sim 1$. In order to compute the mutual impedance response at low frequencies we need first to evaluate the function ϕ/ϕ_0 which is derived from (23) and (27) as

$$\frac{\phi}{\phi_0} = 1 + \sum_{|n|}^{\infty}\frac{b_n}{z_{c_n}} - \frac{2}{\pi}\sum_{|n|}^{\infty}\frac{b_n}{z_{c_n}}\int_0^{\infty}\frac{\sin x\,dx}{x + K_n\rho}, \quad \text{(A7)}$$

where the excitation coefficient, obtained from (24) and (27) by using the properties of the function Z and its derivatives, is

$$\frac{b_n}{z_{c_n}} = \frac{1}{\frac{2z_{c_n}^2}{\tau}\left[1 - \frac{\tau+\mu}{\Omega^2(1+\mu)}\right] - 3 + \frac{2z_{c_n}^4(\tau-1)}{\tau\Omega^2(1+\mu)}Z'(z_{c_n})}. \quad \text{(A8)}$$

When τ tends to 1, the denominator in (A8) becomes simply $(2z^2\varepsilon_c - 3)$, which is the same expression as for a single Maxwellian [*Béghin*, 1995], and this is true whatever μ may be. One can check that the same is true for any finite value of τ, when we set $\mu = 0$ in the dispersion equation (24) and in (A8). This demonstrates that the problem reverts to the one with a single Maxwellian distribution if both populations have the same temperature or if the density of the hot population is zero.

[58] The solution of the dispersion equation (24) at $\Omega_h = 1$ for the two evanescent poles z_{-2} and z_2 is quite easy to obtain analytically since z_c and Z' are purely imaginary. We use the usual Landau wave approximation in order to evaluate the real parts of their contributions to the last right-hand term of (A7) as we did in the single Maxwellian case [*Béghin*, 1995]. This is

$$\Delta\left(\frac{\phi}{\phi_0}\right)_{z_{|2|}} \approx -2\frac{b_{-2}}{z_{-2}}\exp - \left|K_{(-2)}\right|\rho;\ (\Omega \approx \Omega_h), \quad \text{(A9)}$$

where $K_{-2} = k_{-2}\,\lambda_{Dc}$ and ρ is the normalized distance $\rho = r/\lambda_{Dc}$.

[59] The last contribution that needs to be considered is that of the high-order waves, which are expected to have large phase velocities. Here we can use the first two terms of the expansion (A1); then we rewrite (24) as

$$\varepsilon_l \approx \varepsilon_c + 4i\sqrt{\pi}\frac{z_c^3}{\Omega_c^2}e^{-z_c^2} + 4i\sqrt{\pi}\frac{z_c^3}{\Omega_c^2}\frac{e^{\left(-z_c^2/\tau\right)}}{\zeta} = 0; \quad (|z| \gg 1), \tag{A10}$$

where $\zeta = \tau^{3/2}/\mu$ is the parameter that determines the transition point between both populations, as we showed in section 5. The above dispersion equation is multivalued because of the exponential terms, as it is for a single Maxwellian [*Derfler and Simonen*, 1969]. The solutions form an infinite series of poles arranged in pairs symmetric with respect to the imaginary axis in a such way that for any pair with subscript q the poles must satisfy the following relationship: $z_q = -z^*_q$. The distribution of these high-order poles in the negative imaginary half plane is now much more complicated than it is with the single Maxwellian, so we will not discuss it in greater detail in this paper. We take note only that all of them obey the following condition deduced from (A10):

$$z_{c_n}^2 \geq \frac{\tau}{\tau - 1}\left[\ln\zeta + i\pi\,\mathrm{sgn}(n)(2|n| - 1)\right]; \quad (|n| \geq 1). \tag{A11}$$

The above equation states that these waves have a phase velocity larger than at least $\sqrt{\ln\zeta}$ times the thermal velocity of the cold population; that is, they involve electrons beyond the transition point. The global contribution of these poles in (A7) can be written as

$$\Delta\left(\frac{\phi}{\phi_0}\right)_{z_{c_{n\geq|3|}}} = -\frac{2}{\pi}\int_0^\infty \sum_{|n|=3}^{\infty} \frac{b_n}{z_{c_n} + \frac{\rho\Omega}{x\sqrt{2}}}\frac{\sin x\,dx}{x}. \tag{A12}$$

Here we consider a low-frequency range such as $\Omega \ll 1$ (e.g., $\Omega_h = 1$) and distances short compared to the wavelengths for the high-order poles, so we can evaluate the integral in (A12) simply as

$$\Delta\left(\frac{\phi}{\phi_0}\right)_{z_{c_{n\geq|3|}}} \approx -\sum_{|n|=3}^{\infty}\frac{b_n}{z_{c_n}}, \frac{\rho\Omega_h}{z_{c_n}\sqrt{2}} \ll 1. \tag{A13}$$

Returning to (A7), we add this result to the contribution of the evanescent poles given by (A9), and finally, we obtain the following approximate expression:

$$\frac{\phi}{\phi_0} \approx 1 + \sum_{-2}^{2}\frac{b_n}{z_{c_n}} - 2\frac{b_{-2}}{z_{-2}}\exp - \left|K_{(-2)}\right|\rho; \quad (\Omega \approx \Omega_h), \tag{A14}$$

which reduces the problem to the relatively simple one of determining the properties of the dominant poles.

[60] **Acknowledgments.** The authors are grateful to L. R. O. Storey and V. Krasnoselkikh for very fruitful remarks and comments and to P. Archambault for his efficient work in the code development. The WHISPER experiment and software were realized thanks to a CNES contract. Portions of this work were carried out under NASA Goddard Space Flight Center grant NNG 04 GB09G, and J.S.P. thanks the Deep Space Network for scheduling and carrying out the WBD operations. The research of D.S. was partially supported by the European Community through contract HPRN-CT-2001-00314, and B.L. acknowledges financial support from the PPARC.

References

Béghin, C. (1995), Series expansion of electrostatic potential radiated by a point source in isotropic Maxwellian plasma, *Radio Sci.*, *30*, 307–322.

Béghin, C. (2002), Review of critical parameters for modeling electric antennas in space plasmas, in *Proceedings of the URSI XXVIIth General Assembly, Maastricht, The Netherlands, 17–24 Aug. 2002* [CD-ROM], paper 1273, IEEE Press, New York.

Béghin, C., and E. Kolesnikova (1998), Surface-charge distribution approach for modeling of quasi-static electric antennas in isotropic thermal plasma, *Radio Sci.*, *33*, 503–516.

Chasseriaux, J. M., R. Debrie, and C. Renard (1972), Electron density and temperature measurements in the lower ionosphere as deduced from the warm plasma theory of the quadrupole probe, *J. Plasma Phys.*, *8*, 231–253.

Chateau, Y. F., and N. Meyer-Vernet (1991), Electrostatic noise in non-Maxwellian plasmas: Generic properties and "kappa" distributions, *J. Geophys. Res.*, *96*, 5825–5836.

Décréau, P. M. E., C. Béghin, and M. Parrot (1978), Electron density and temperature as measured by the mutual impedance experiment on board GEOS-1, *Space Sci. Rev.*, *22*, 581–595.

Décréau, P. M. E., et al. (1997), WHISPER, a resonance sounder and wave analyser: Performances and perspectives for the Cluster mission, *Space Sci. Rev.*, *79*, 157–193.

Derfler, H., and T. C. Simonen (1969), Higher-order Landau modes, *Phys. Fluids*, *12*, 269–278.

Feldman, W. C., et al. (1982), Electron heating within the Earth's bow shock, *Phys. Rev. Lett.*, *49*, 199–201.

Fried, B. D., and S. D. Conte (1961), *The Plasma Dispersion Function: The Hilbert Transform of the Gaussian*, Elsevier, New York.

Geiswiller, J., C. Béghin, E. Kolesnikova, D. Lagoutte, J. L. Michau, and J. G. Trotignon (2001), Rosetta spacecraft influence on the mutual impedance probe frequency response in the long Debye length mode, *Planet. Space Sci.*, *49*, 633–644.

Génot, V., and S. Schwartz (2004), Spacecraft potential effects on electron moments derived from a perfect plasma detector, *Ann. Geophys.*, *22*, 2073–2080.

Gurnett, D. A., R. L. Huff, and D. L. Kirchner (1997), The wide-band plasma wave investigation, *Space Sci. Rev.*, *79*, 195–208.

Gustafsson, G., et al. (1997), The electric field and wave experiment for the Cluster mission, *Space Sci. Rev.*, *79*, 137–150.

Johnstone, A. D., et al. (1997), PEACE: A Plasma Electron and Current Experiment, *Space Sci. Rev.*, *79*, 351–398.

Kolesnikova, E., and C. Béghin (2001), Instability problem of the electric field antennas on the Polar spacecraft, *Radio Sci.*, *36*, 203–222.

Maksimovic, M., et al. (1995), Solar wind electron parameters from quasi-thermal noise spectroscopy and comparison with other measurements on Ulysses, *J. Geophys. Res.*, *100*, 19,881–19,891.

Meyer, P., and N. Vernet (1975), The impedance of a dipole antenna in the ionosphere: 2. Comparison with theory, *Radio Sci.*, *10*, 529–536.

Meyer-Vernet, N., and C. Perche (1989), Tool kit for antennae and thermal noise near the plasma frequency, *J. Geophys. Res.*, *94*, 2405–2415.

Pedersen, A., et al. (1997), The Wave Experiment Consortium (WEC), *Space Sci. Rev.*, *79*, 93–105.

Pedersen, A., F. Mozer, and G. Gustafsson (1998), Electric field measurements in a tenuous plasma with spherical double-probes, in *Measurement Techniques in Space Plasma: Fields*, *Geophys. Monogr. Ser.*, vol. 103, edited by R. F. Pfaff, J. E. Borovsky, and D. T. Young, pp. 1–12, AGU, Washington, D. C.

Perraut, S., H. de Feraudy, A. Roux, P. M. E. Décréau, J. Paris, and L. Matson (1990), Density measurements in key regions of the Earth magnetosphere: Cusp and auroral region, *J. Geophys. Res.*, *95*, 5997–6014.

Storey, L. R. O. (1998), Mutual-impedance techniques for space plasma measurements, in *Measurement Techniques in Space Plasma: Fields*, *Geophys. Monogr. Ser.*, vol. 103, edited by R. F. Pfaff, J. E. Borovsky, and D. T. Young, pp. 155–160, AGU, Washington, D. C.

C. Béghin, P. M. E. Décréau, and D. Sundkvist, CNRS, 3A Av. de la Recherche Scientifique, F-45071, Orléans Cedex 2, France. (cbeghin@cnrs-orleans.fr)

B. Lefebvre, The Blackett Laboratory, Imperial College London, London SW7 2BW, UK.

J. Pickett, Department of Physics and Astronomy, 203 Van Allen Hall, University of Iowa, Iowa City, IA 52242-1942, USA.